ACS APPLIED MATERIALS & INTERFACES

Research Article

www.acsami.org

Growth of Highly Conductive Ga-Doped ZnO Nanoneedles

Yu-Feng Yao, Charng-Gan Tu, Ta-Wei Chang, Hao-Tsung Chen, Chi-Ming Weng, Chia-Ying Su, Chieh Hsieh, Che-Hao Liao, Yean-Woei Kiang, and C. C. Yang*

Institute of Photonics and Optoelectronics, and Department of Electrical Engineering, National Taiwan University, 1, Roosevelt Road, Section 4, Taipei 10617, Taiwan

ABSTRACT: The molecular beam epitaxy growth of highly degenerate Ga-doped ZnO (GaZnO) nanoneedles (NNs) based on the vapor−liquid−solid (VLS) growth mode using Ag nanoparticles (NPs) as the growth catalyst is demonstrated. It is shown that when the growth substrate temperature is sufficiently high, a portion of a Ag NP can be melted for serving as the catalyst to precipitate GaZnO on the residual Ag NP and form a GaZnO NN. Record-low turn-on and threshold electric fields in the field emission test of the grown GaZnO NNs are observed. Also, a record-high field enhancement factor in field emission is calibrated. Such superior field emission performances are attributed to a few factors, including (1) the low work function and high conductivity of the grown GaZnO NNs due to highly degenerate Ga doping, (2) the sharp-pointed geometry of the vertically aligned GaZnO NNs, (3) the Ag doping in VLS precipitation of GaZnO for further reducing NN resistivity, and (4) the residual small Ag NP at the NN tip for making the tip even sharper and tip conductivity even higher.

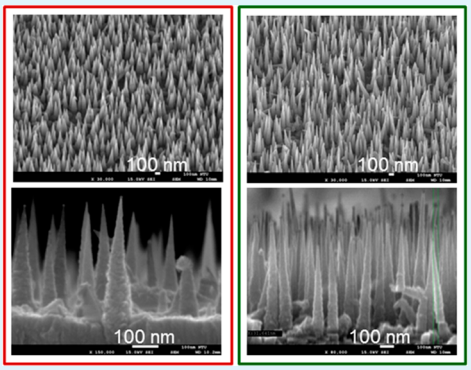

KEYWORDS: *Ga-doped ZnO, nanoneedle, vapor−liquid−solid mode, growth catalyst, field emission*

1. INTRODUCTION

Due to their desirable properties of electrical conductivity and optical transparency, transparent conducting oxides (TCOs) have been widely investigated for the applications to optoelectronic devices, including solar cell, liquid crystal display, and light-emitting diode. Generally, a TCO thin film exhibits a resistivity level lower than 10^{-3} Ω-cm and an average transmittance over 80% in the visible range. The high optical transparency in the visible range is attributed to its large band gap energy (>3 eV). The high electrical conductivity in a TCO can be achieved by introducing certain native defects (e.g., oxygen vacancies) or by doping certain impurities. Generally, a TCO thin film has a polycrystalline or amorphous structure.[1] Nowadays, the electron concentrations in well-developed TCOs vary from 10^{20} to 10^{21} cm^{-3}.[2−4] Although indium tin oxide (ITO) is currently the most widely used TCO, the development of other TCOs is desirable because of the high cost of ITO and the scarcity of indium. In this regard, impurity-doped ZnO, such as Al-doped ZnO (AlZnO)[5,6] and Ga-doped ZnO (GaZnO),[7,8] is promising. The electron concentrations and resistivity levels of the reported highly doped ZnO can be higher than 6×10^{20} cm^{-3} and lower than 3×10^{-4} Ω cm, respectively. The key factors for reaching high electron concentration and low resistivity in GaZnO include low growth temperature (200−400 °C), high Ga content (4−8%), and polycrystalline structure.[9,10]

On the basis of the physical phenomenon of quantum tunneling, in a field emission process, electrons are injected from the surface of a material structure into a vacuum driven by an applied electric field. Such a process is described by the Fowler−Nordheim equation as[11,12]

$$J = A_E \frac{\beta^2 E^2}{\phi} \exp\left(\frac{-B_E \phi^{3/2}}{\beta E}\right) \quad (1)$$

Here, J is the emitted current density, E is the applied electric field, ϕ is the material work function, β is the field enhancement factor, $A_E = 1.56 \times 10^{-10}$ (A eV)/V^2, and $B_E = 6.83 \times 10^3$ V/($eV^{3/2}$ μm). The Fowler−Nordheim equation predicts that by using a material structure with a low work function and high field enhancement factor, field emission current density can be greatly enhanced. The field enhancement factor is defined as the ratio of the local electric field at the emission spot to the applied electric field. It is useful for evaluating the degree of field emission enhancement of a tip structure over a flat surface. For a nanostructured emitter, a high β value can be achieved by designing a high aspect ratio in geometry and a high curvature at the emitting tip, and by using a material of high conductivity.

Two approaches have been used for improving field emission efficiency through tuning the work function of a material. First, metal nanoparticles (NPs) are decorated to achieve a lower work function.[13,14] Second, doping with impurities can change the work function.[12,15] In particular, n-type doping can raise the Fermi energy level of a material for effectively reducing its work

Received: March 9, 2015
Accepted: April 30, 2015
Published: April 30, 2015

DOI: 10.1021/acsami.5b02063
ACS Appl. Mater. Interfaces 2015, 7, 10525−10533

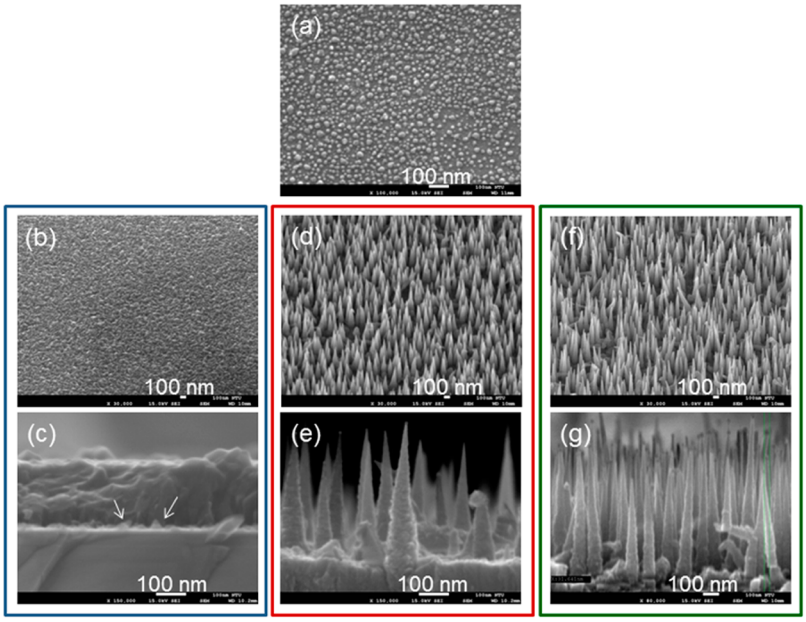

Figure 1. (a) Tilted SEM image of Ag NPs on a GaN template. (b, c) Tilted and cross-sectional SEM images, respectively, of the GaZnO growth result when the growth substrate temperature is 250 °C. (d, e) Tilted and cross-sectional SEM images, respectively, of the GaZnO growth result when the growth substrate temperature is 350 °C. (f, g) Tilted and cross-sectional SEM images, respectively, of the GaZnO growth result when the growth substrate temperature is 450 °C.

function. Also, doping can reduce its resistivity through the increase of carrier concentration, and thus the decrease the voltage drop in the material, resulting in the enhancement of the electric field at the emission tip, i.e., increasing β. In this situation, negative electron affinity can be achieved through heavy doping for extremely effective field emission.[16] In the past, field emission study has been focused on carbon nanotubes,[17−19] graphene,[20−22] and other materials of low work functions.[23−25] Recently, ZnO nanostructures for field emission application have attracted much attention due to their high thermal stability, oxidation resistance in harsh environments, and controllable electronic characteristics.[26−28] N-type doping in ZnO for enhancing field emission efficiency has been reported.[12,15] In particular, ZnO nanostructures, either undoped or Al-, In-, or Ga-doped, have been widely used for field emission application.[12,15,29−34] However, due to the low doping concentrations, their turn-on electrical fields were generally larger than 2 V/μm, and the field enhancement factors were generally smaller than 10^4. The performance of field emission can be significantly improved if the electron concentration of a ZnO nanostructure can be largely increased. Generally speaking, the doping levels in those reports did not reach the condition of degenerate carrier concentration (>5 × 10^{20} cm^{-3}) in ZnO. Due to their high growth temperature (>450 °C), single-crystal structures with low Ga incorporations (<1%) were formed. The conductivity of such a ZnO structure is not high enough for effective field emission application.

Various methods have been developed for fabricating one-dimensional ZnO nanostructures, including a hydrothermal process, thermal evaporation, vapor-phase transport, atomic layer deposition, chemical vapor deposition, metalorganic chemical vapor deposition (MOCVD), pulsed laser deposition, and molecular beam epitaxy (MBE). To form a nanowire or nanoneedle (NN) structure for effective field emission application, the vapor−liquid−solid (VLS) growth mode with catalytic metal NPs has been proven to be a useful approach.[35−37] In particular, oriented NNs of a higher doping concentration can be obtained when a better controlled growth technique, such as MOCVD or MBE, is used. In the VLS growth process, the target material atoms (vapor) are first absorbed by the melting catalytic metal NP (liquid). When the supersaturation condition is reached, the target material crystal (solid) is precipitated from the bottom of the metal NP on a crystal-compatible substrate. In this paper, we demonstrate the MBE growth of GaZnO NNs based on the VLS growth mode using Ag NPs as growth catalyst. When the growth substrate temperature is sufficiently high, a portion of a Ag NP can be melted for serving as the catalyst to precipitate GaZnO on the residual Ag NP and form a GaZnO NN. The grown GaZnO NNs are used for demonstrating record-low turn-on and threshold electric fields and record-high field enhancement factor in a field emission test. The superior field emission behaviors are attributed to a few factors, including (1) the low work function (<4.2 eV) and high conductivity of the grown GaZnO NNs due to highly degenerate Ga doping, (2) the sharp-pointed geometry of the vertically aligned GaZnO NNs, (3) the Ag doping in VLS precipitation of GaZnO for further reducing NN resistivity, and (4) the residual small Ag NP at the NN tip for making the tip even sharper and tip conductivity even higher. The Ag doping in GaZnO and the formation of a Ag NP at the NN tip are achieved naturally through the VLS growth of GaZnO NNs. In section 2 of this paper, the growth process of GaZnO NNs is described. The characterization results of the GaZnO NNs are presented in section 3. The growth mechanism of GaZnO NNs is discussed in section 4. Then, the results of field emission tests are reported in section 5. Finally, conclusions are drawn in section 6.

2. GROWTH OF GaZnO NANONEEDLES

The formation of GaZnO NNs is based on the VLS growth mode using Ag NPs as growth catalyst on a *c*-plane GaN template, which is deposited on sapphire substrate with

DOI: 10.1021/acsami.5b02063
ACS Appl. Mater. Interfaces 2015, 7, 10525−10533

metalorganic chemical vapor deposition. A *c*-plane GaN template is chosen because it has a similar lattice size to that of ZnO such that the *c*-axis growth of NNs in the VLS mode can follow the vertical direction for forming vertical and parallel NNs. Figure 1a shows the tilted scanning electron microscopy (SEM) image of Ag NPs on the GaN template. The Ag NPs are formed by first depositing a Ag layer of 1.5 nm in thickness on GaN followed by a thermal annealing process at 300 °C for 30 min with ambient nitrogen. The planar dimension of Ag NPs ranges from 15 to 50 nm, with an average size around 25 nm. GaZnO is grown with an RF-plasma assisted MBE reactor under the Zn-rich conditions of 320 °C in Zn effusion cell temperature, 900 °C in Ga effusion cell temperature, 1 sccm in O_2 flow rate, and 350 W in RF-plasma power. Three substrate temperatures are used for growing GaZnO on the GaN template with Ag NPs. Figure 1b,c shows the tilted and cross-sectional SEM images, respectively, of the growth results when the substrate temperature is 250 °C and the growth duration is 60 min. In this situation, one can see that a GaZnO thin film of ∼240 nm in thickness is formed on the template with the Ag NPs buried at the bottom. Two of the buried Ag NPs are indicated by the two arrows in Figure 1c. Then, the substrate temperature of MBE growth is raised to 350 °C to give the growth results shown in Figure 1d,e when the growth duration is 80 min. As shown in Figure 1d for a tilted SEM image, NNs are formed on the sample surface. In Figure 1e for a cross-sectional SEM image, one can see that NNs of ∼400 nm in height are formed on a thin film of ∼165 nm in thickness. The comparison between Figure 1b,c and Figure 1d,e indicates that the substrate temperature of MBE growth must be sufficiently high for NN formation. Next, the substrate temperature of MBE growth is further raised to 450 °C to give the growth results shown in Figure 1f,g when the growth duration is 80 min. In this situation, NNs are also formed on a thin film. With the growth at 450 °C, the heights of the NNs become larger in the range 850−950 nm.

To confirm GaZnO growth, energy-dispersive X-ray spectroscopy (EDX) analysis is undertaken at a few positions on an NN and the simultaneously grown thin film in either sample grown at 350 or 450 °C. As indicated in the transmission electron microscopy (TEM) images in Figure 2a,b for the NN samples grown at 350 and 450 °C, respectively, the Ga compositions at nine points in either sample are measured. The atomic percentages of Ga at those nine points in both samples are listed in Table 1. Here, one can see that the Ga atomic composition varies from 4.72% to 7.58% (from 1.95% to 5.65%) in the NN and the thin film in the sample grown at 350 °C (450 °C). The average Ga atomic composition over the nine points in the sample grown at 350 °C (5.90%) is significantly larger than that in the sample grown at 450 °C (4.12%). Such results confirm the growth of GaZnO NNs with a simultaneously grown GaZnO thin film when the MBE substrate temperature is higher than or equal to 350 °C. Also, a higher growth temperature leads to lower Ga incorporation in either an NN or the thin film.

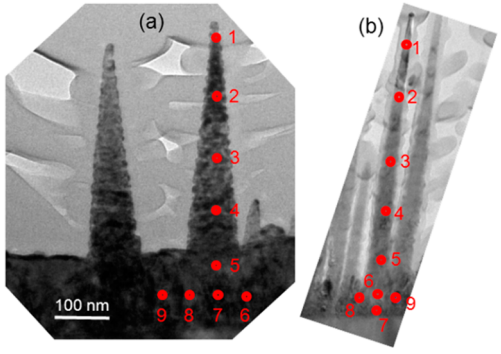

Figure 2. (a) TEM image of two GaZnO NNs grown at 350 °C for showing the nine positions of EDX measurement to give Ga compositions. (b) TEM image of a GaZnO NN grown at 450 °C for showing the nine positions of EDX measurement to give Ga compositions.

3. CHARACTERIZATION OF GaZnO NANONEEDLES

To understand the crystal structure of the GaZnO NNs, the diffraction patterns of atomic-scale TEM images near the top and middle height of a GaZnO NN grown at 350 °C are analyzed. Figure 3a repeats the cross-sectional TEM image of the right NN in Figure 2a to indicate the two positions for diffraction pattern analysis. Figure 3b,c shows the atomic-scale TEM images around the two assigned positions on the GaZnO NN. Figure 3d,e [Figure 3f,g] shows the diffraction patterns of the two square areas shown in Figure 3b [Figure 3c]. In each set of diffraction patterns, the orientations of the (002) crystal directions are indicated with the dashed lines. Those dashed lines are repeated in the inset for the comparison between the two diffraction patterns. Here, one can see that the two (002) orientations in parts d and e in Figure 3 deviate from each other by ∼3°. However, those in parts f and g in Figure 3 are almost parallel. Such results imply that a GaZnO NN has a multicrystal structure with crystal orientation that varies slightly from domain to domain. The formation of multicrystal in the VLS mode is mainly caused by the low-temperature growth. Normally, at a high temperature, a single-crystal nanostructure can be obtained with VLS growth. In the case of GaZnO nanowire growth, VLS growth can result in the precipitation of single-crystal GaZnO at a high temperature (>500 °C). However, in this situation, Ga content is quite low. At the used low temperatures (<500 °C), Ga content can be significantly increased. In particular, with Zn-rich growth, Ga incorporation becomes even stronger. In this situation, multicrystal GaZnO is formed with a domain size 15−20 nm. This is true in both planar and VLS growths. It has been reported that, with such a domain structure, the defects (e.g., oxygen vacancies) at domain boundaries can increase electron concentration in GaZnO for assisting carrier tunnelling through domain boundaries, leading to high carrier mobility in GaZnO.[38] In a TEM image, small dark spots can be seen at the tips of GaZnO NNs. Such dark spots correspond to the residual catalytic Ag NPs. During the VLS growth process, catalytic metal atoms can mix into the precipitated material leading to the size shrinkage of the catalytic metal NP. Figure 4a shows a TEM image of three GaZnO NNs grown at 350 °C to indicate the two positions for Ag content analysis. The atomic-scale TEM images around these two positions, one at the tip and the other at the bottom of the NN, are shown in Figure 4b,c, respectively. In either part b or part c of Figure 4, fringe patterns with a lattice constant of 0.239 nm can be clearly seen. This lattice constant corresponds to Ag (111) crystal face, indicating the high Ag contents at these two positions. Figure 4d,e shows the corresponding EDX spectra, confirming their high Ag contents. The Ag atomic percentages are estimated to be 90% and 75% at the NN top and bottom, respectively. The relatively lower percentage of Ag content at the NN bottom is

DOI: 10.1021/acsami.5b02063
ACS Appl. Mater. Interfaces 2015, 7, 10525−10533

Table 1. Ga Atomic Percentages from EDX Measurements at those Positions shown in Figure 2a,b for the NN Samples Grown at 350 and 450 °C, Respectively

	position									
	1	2	3	4	5	6	7	8	9	av
350 °C	7.58	5.67	4.82	6.58	5.98	5.96	4.72	6.15	5.61	5.90
450 °C	4.96	5.65	1.95	3.73	4.05	5.34	3.65	3.18	4.57	4.12

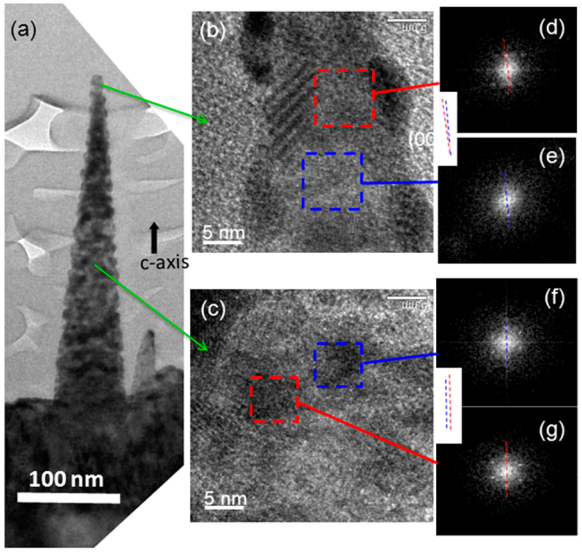

Figure 3. (a) TEM image of a GaZnO NN grown at 350 °C for showing the two positions of crystal orientation analysis. (b, c) Atomic-scale TEM images around the two designated positions. (d, e) Diffraction patterns of the two square areas shown in part b. (f, g) Diffraction patterns of the two square areas shown in part c. In each set of diffraction patterns, the orientations of the (002) crystal directions are indicated with the dashed lines. Those dashed lines are repeated in the inset for comparison.

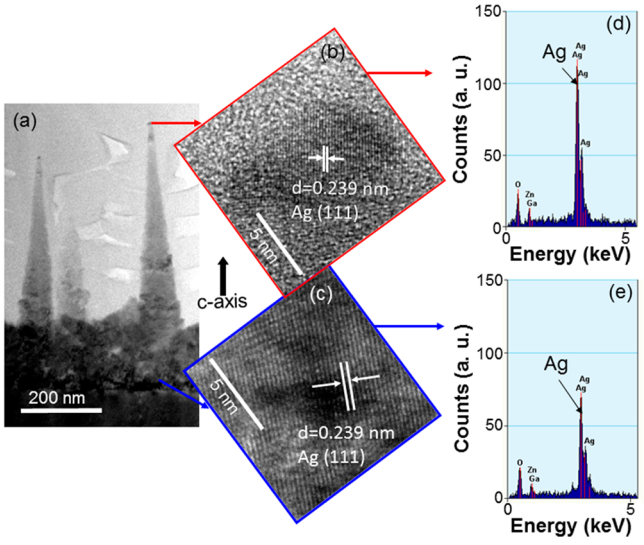

Figure 4. (a) TEM image of three GaZnO NNs grown at 350 °C to indicate the two positions for Ag content analysis. (b, c) Atomic-scale TEM images at these two positions. (d, e) Corresponding EDX spectra at the two positions, indicating their high Ag contents.

due to the thicker sample there, in which a possibly existent Ag NP is surrounded by GaZnO. The observed Ag content at the bottom of a GaZnO NN may be caused by Ag NPs nearby, which are not involved in the VLS growth. However, it can also be due to the incomplete use of the Ag NP, which is involved in the VLS growth of the NN above. It is noted that corrugation structures can be seen on the GaZnO NN shown in Figure 3a. The formation of such a corrugation structure can be related to the multicrystal precipitation of GaZnO. However, its formation mechanism requires further investigation.

As mentioned earlier, Ag atoms can mix into the precipitated GaZnO during the VLS growth process of an NN. In the TEM image of Figure 5a, we show a GaZnO NN grown at 350 °C with a vertical (red) arrow drawn along the NN for EDX scan. Figure 5b shows the line-scan Ag contents with the Ag-L and Ag-K lines. Here, the horizontal (red) arrow at the top indicates the EDX scan direction following that in Figure 5a. In Figure 5b, one can see the generally decreasing trend of Ag content along the NN height. The short (blue) arrows in Figure 5a,b show the location of the NN tip, at which a small Ag NP leads to a clear feature of Ag content. It is noted that the line scan shown in Figure 5a may pass another Ag NP at the NN bottom. This Ag NP may result in one of the features in the data of the Ag-L and Ag-K lines toward the right end of Figure 5b. However, it is difficult to identify this feature. Figure 5c shows the same TEM image as Figure 5a. However, now a horizontal (red) arrow in the GaZnO thin film is drawn for EDX scan. Figure 5d shows the corresponding line-scan Ag contents with the Ag-L and Ag-K lines. Here, again, the horizontal (red) arrow at the top indicates the EDX scan direction following that in Figure 5c. The short (blue) arrows in Figure 5c,d show the position of the NN portion buried in the GaZnO thin film. In Figure 5d, one can see a clear feature in either Ag-L or Ag-K line at this position. This Ag feature can originate either from the Ag content in the GaZnO NN or from a residual Ag NP there. It is noted that the Ag content outside the NN is negligibly small in the GaZnO thin film. From the results in Figure 5b,d, one can conclude that Ag atoms exist in a GaZnO NN, which is grown through the VLS mode with catalytic Ag, but not in the simultaneously grown GaZnO thin film, which is formed through the ordinary two-dimensional growth.

4. GROWTH MECHANISM OF GaZnO NANONEEDLES

To understand the growth mechanism of GaZnO NNs, we investigate their early stage growth behaviors. Figure 6a–d shows tilted SEM images of GaZnO growth results on GaN templates with Ag NPs at 350 °C for 10, 20, 30, and 40 min, respectively. In Figure 6a, one can see that GaZnO emerges from some of the Ag NPs to show the bright spots. Generally, GaZnO is formed only from those Ag NPs of relatively smaller sizes. In this stage, a thin GaZnO film is also formed to slightly cover those Ag NPs of larger sizes. In Figure 6a, a typical Ag NP with emergent GaZnO is indicated by an arrow. The basal width and height of this structure (Ag NP plus GaZnO NN) are estimated to give 36 and 118 nm, respectively. When the VLS growth time increases to 20 min, the structure size of the Ag NP plus GaZnO NN becomes larger, as shown in Figure 6b. In this situation, the basal width and height of a typical

DOI: 10.1021/acsami.5b02063
ACS Appl. Mater. Interfaces 2015, 7, 10525−10533

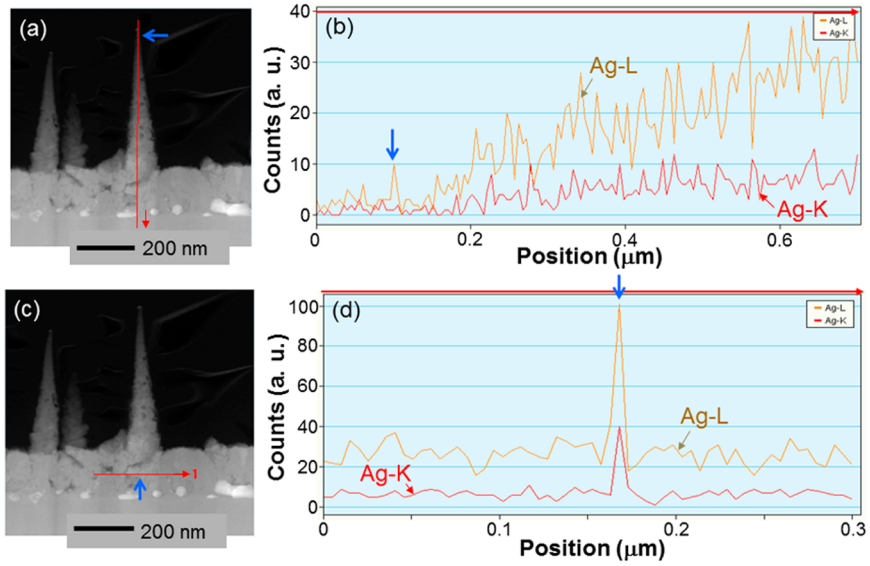

Figure 5. (a) TEM image of GaZnO NNs grown at 350 °C with a vertical (red) arrow along an NN drawn for EDX scan. (b) Line-scan Ag contents with the Ag-L and Ag-K lines. Here, the horizontal (red) arrow at the top shows the scan direction following that in part a. The short (blue) arrows in parts a and b indicate the location of the NN tip, at which a small Ag NP leads to a clear feature of Ag content. (c) Same TEM image as in part a with a horizontal (red) arrow in the GaZnO thin film drawn for EDX scan. (d) Corresponding line-scan Ag contents with the Ag-L and Ag-K lines. The short (blue) arrows in parts c and d indicate the position of the GaZnO NN portion buried in the thin film.

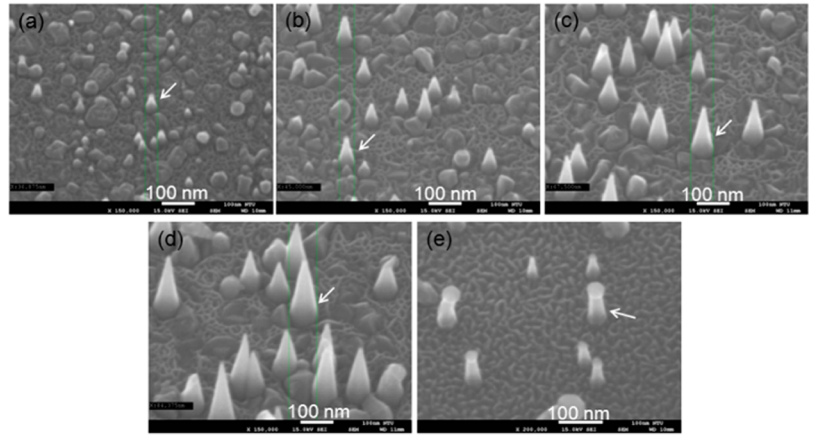

Figure 6. (a–d) Tilted SEM images of GaZnO growth results at 350 °C on GaN templates with Ag NPs as catalyst for 10, 20, 30, and 40 min, respectively. (e) Tilted SEM image of GaZnO growth result at 450 °C on a GaN template with Ag NPs as catalyst for 10 min.

structure, as indicated by the arrow, are estimated to give 45 and 184 nm, respectively. The basal width and height of the structure including Ag NP and GaZnO NN indicated by the arrow when the VLS growth time is 30 (40) min shown in Figure 6c [Figure 6d] are increased to 67 and 312 nm (84 and 393 nm), respectively. As VLS growth time increases, the GaZnO thin film filling the space between GaZnO NNs becomes thicker and thicker and eventually covers the Ag NPs completely. It is noted that the basal width of the structure including Ag NP and GaZnO NN becomes larger than the original Ag NP size after VLS growth.

Figure 7a shows the TEM image of a few GaZnO NNs when the VLS growth time is 10 min at 350 °C. Here, one can see that a small Ag NP exists at the top of each GaZnO NN, indicating that the VLS growth for forming the GaZnO NNs is based on the catalytic reaction of the small Ag NP at the NN tip. Figure 7b shows the TEM image of two GaZnO NNs when the VLS growth time is 20 min at 350 °C. Atomic compositions at the three positions marked on the proximal NN are

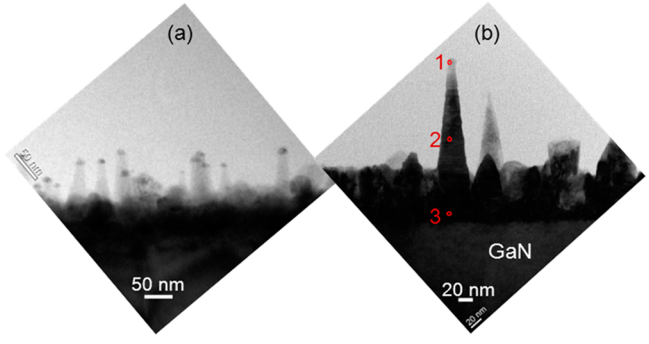

Figure 7. (a) TEM image of GaZnO NNs grown at 350 °C for 10 min to show the Ag NPs at the NN tips. (b) TEM image of two GaZnO NNs grown at 350 °C for 20 min with three designated positions for EDX measurement.

evaluated with EDX to give the results in Table 2. Here, at the NN top and bottom (points 1 and 3, respectively), high Ag

DOI: 10.1021/acsami.5b02063
ACS Appl. Mater. Interfaces 2015, 7, 10525–10533

Table 2. Atomic Compositions of Zn, Ga, and Ag at the Three Positions Shown in Figure 7b

	position		
	1	2	3
Zn (%)	5.98	94.41	84.42
Ga (%)	16.60	4.81	5.88
Ag (%)	77.42	0.87	14.97

compositions are observed, indicating the existence of Ag NPs at these two positions. The relatively lower Ag composition at point 3 is due to the burial of the Ag NP there by a thick GaZnO layer. The relatively larger Ga composition at point 1 can be attributed to the rich Ga absorption by the catalytic Ag NP.

The growth scenarios of a GaZnO NN from a catalytic Ag NP are schematically demonstrated in Figure 8. At the beginning, as shown at the left end, a Ag NP of a reasonably small size can be partly melted as the substrate temperature of MBE growth is raised to a certain level. Here, the melting portion of the Ag NP is presented with the lighter gray color. Only this melting portion of the Ag NP serves as the catalyst for VLS growth. GaZnO is precipitated from the bottom of this melting Ag NP portion, resulting in the growth of GaZnO on the inactive Ag NP portion at the bottom and the push-up of the catalytic Ag NP. In a conventional VLS process for growing a semiconductor nanostructure, the semiconductor material precipitates from the bottom of the whole catalytic metal NP to form a nanostructure on a template, which usually is a material allowing target material overgrowth, when the template temperature is high enough for melting the whole metal NP. If such a temperature is not reached, the VLS growth behavior cannot be observed. However, because GaZnO can be grown on a metal,[39] it can be precipitated between the melting and unmelting portions of a Ag NP, leading to the result shown in Figures 6a and 8. As shown in Figure 1b,c, when the substrate temperature is 250 °C, the temperature is not high enough for melting a significant portion of a Ag NP for producing a VLS growth effect such that the GaZnO growth simply forms a thin film covering the Ag NPs. As the substrate temperature is increased to 350 °C, those Ag NPs of relatively smaller sizes can be partly melted for the VLS growth results shown in Figure 6a–d. At 350 °C, the Ag NPs of larger sizes cannot be effectively melted for generating a VLS growth effect. Therefore, only the smaller Ag NPs result in the growth of GaZnO NNs. The Ag NPs of larger sizes can be used for GaZnO NN growth when the substrate temperature is further increased. Figure 6e shows the tilted SEM image of a sample after 10 min growth at 450 °C on a Ag NP template. Here, a Ag NP at the top of a GaZnO NN can be clearly seen. It is noted that the size of the top Ag NP (~40 nm) in the sample grown at 450 °C shown in Figure 6e is significantly larger than that (~15 nm) in the sample grown at 350 °C shown in Figure 6a. At the higher growth temperature, a larger portion of a Ag NP or the whole Ag NP can be melted for producing the VLS growth effect. Also, larger Ag NPs can be involved in VLS growth. However, as growth temperature increases, Ga content is reduced, as indicated in Table 1. In this situation, the electrical property is degraded.[9,10] As shown in Figure 6a–d, the basal width of a GaZnO NN grown at 350 °C increases with growth time and eventually becomes larger than the planar size of the original Ag NP. The increasing basal width of a NN can be attributed to the GaZnO precipitation in a planar area larger than the size of the catalytic Ag NP at the top during the VLS process. It can also be due to the VLS growth through the melting side-surface of the residual Ag NP at the NN bottom before it is covered by the simultaneously grown GaZnO thin film, which is deposited without the VLS process. Without the VLS process, no Ag content can be found in the GaZnO thin film, as shown in Figure 5d. In Figure 8, we use slightly different colors to differentiate the GaZnO portion with Ag doping from that without Ag doping. As schematically shown in Figure 8, the Ag NP at the tip of the NN becomes smaller and smaller along the VLS growth due to the Ag doping into the GaZnO NN.

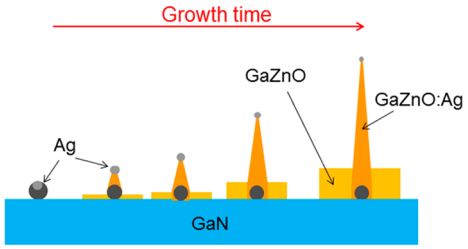

Figure 8. Schematic demonstration of the growth scenarios of a GaZnO NN from a catalytic Ag NP.

5. FIELD EMISSION BEHAVIOR OF GaZnO NANONEEDLES

In the field emission test of the grown GaZnO NNs, the GaZnO thin film is used as the cathode. The anode is made of copper. The distance between the cathode and anode surfaces is 120 μm. The test area is 0.9 cm × 0.9 cm. The pressure of the vacuum chamber for electron emission is 5×10^{-7} Torr. A voltage source (Keithley 2410) is used for the field emission measurement. Figure 9 shows the emission current density (J) as a function of applied electric field (E) for the NN sample grown at 350 °C. For comparison, in the inset of Figure 9, besides the emission current density as a function of applied electric field for the NN sample grown at 350 °C, the similar result for the NN sample grown at 450 °C is shown. In Figure 10, we show the values of $\ln(J/E^2)$ as functions of $1/E$ for the NN samples grown at 350 and 450 °C. Two straight dashed

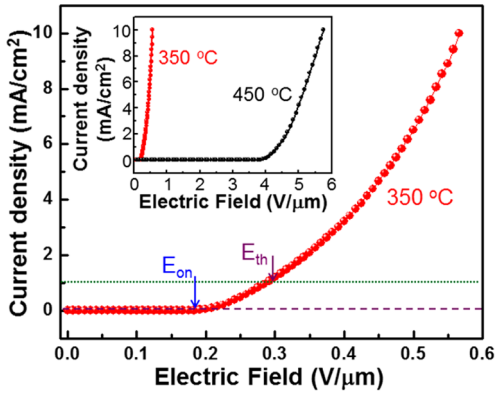

Figure 9. Emission current density as a function of applied electric field in field emission test of the GaZnO NN sample grown at 350 °C. The definitions of the turn-on electric field, E_{on}, and threshold electric field, E_{th}, are demonstrated. In the inset, besides the result of the sample grown at 350 °C, the similar result of the sample grown at 450 °C is shown for comparison.

DOI: 10.1021/acsami.5b02063
ACS Appl. Mater. Interfaces 2015, 7, 10525–10533

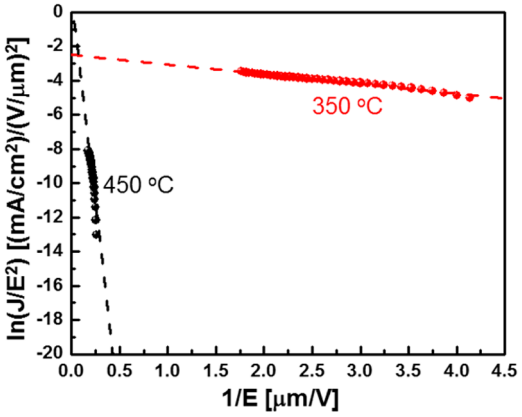

Figure 10. Values of $\ln(J/E^2)$ as functions of $1/E$ for the NN samples grown at 350 and 450 °C.

lines are drawn for fitting the data curves. According to the Fowler–Nordheim equation, such a curve must be a straight line. The two quasilinear curves in Figure 10 confirm that the field emission behaviors follow the Fowler–Nordheim equation. For describing the field emission behavior, the turn-on electric field (E_{on}) and threshold electric field (E_{th}) are usually defined as the applied electric fields for the emission current density to reach 10 μA/cm^2 and 1 mA/cm^2, respectively.[40] The values of those defined electric fields for the NN sample grown at 350 °C are listed in column 6 of Table 3. Here, one can see that E_{on} and E_{th} are as small as 0.18 and 0.3 V/μm, respectively. From the results in Figure 9, by assuming that the work function of GaZnO is 4.2 eV,[41] based on eq 1, we can evaluate the field enhancement factor, β, of the NN sample grown at 350 °C to give 5.0 × 10^4.[11,12] The work function assumption of 4.2 eV is based on the highly degenerate Ga doping into ZnO such that its Fermi level can be lifted to become coincident with or even higher than the conduction band-edge. The value of 4.2 eV corresponds to the potential difference between the vacuum level and the conduction band-edge of ZnO. The evaluated β value is also shown in column 6 of Table 3. The corresponding field emission results of the NN sample grown at 450 °C are listed in column 7 of Table 3. With lower Ga doping in this sample, its work function is estimated to be 5.3 eV.[12] Here, one can see that the turn-on electric field is increased to 3.83 V/μm and the field enhancement factor is reduced to 2072. Columns 2–5 of Table 3 show the related results of three representative materials, which have been developed for field emission application, including graphene,[20] carbon nanotube (CNT) coated with Ag NPs for reducing its effective work function,[13] neodymium hexaboride (NdB_6, which has a low work function at 1.6 eV),[25] and ZnO NNs.[27] From the comparisons shown in Table 3, one can see that either the turn-on or threshold electric field of our GaZnO NNs grown at 350 °C is lower, when compared with other reported materials. Also, the field enhancement factor of our GaZnO NNs grown at 350 °C is higher than those of the other four materials. As a matter of fact, through literature survey, it is found that the turn-on and threshold electric fields of this work are the lowest ever reported. Meanwhile, the field enhancement factor of this work is the highest ever reported.

The low turn-on and threshold electric fields and high field enhancement factor in the field emission test of the GaZnO NN sample grown at 350 °C are mainly due to the highly degenerate Ga doping into ZnO. In this situation, the Fermi level can be lifted to become coincident with or even higher than its conduction band-edge such that the work function is reduced (<4.2 eV) for effective electron emission. Also, the material resistivity is reduced for focusing the voltage drop at the NN tip and hence increasing the field enhancement factor. Meanwhile, the sharp NN tip (<10 nm) also helps in increasing the field enhancement factor. In particular, the small Ag NP at the NN top makes the tip even sharper and increases the electron concentration at the tip. Besides, the vertically aligned NN geometry helps in increasing the field emission efficiency. In addition, the Ag doping during VLS precipitation can further reduce the material resistivity. It is noted that Ag doping in ZnO under the O-rich growth condition for Ag atoms to occupy Zn sites and hence for forming p-type ZnO has been reported.[42,43] However, GaZnO is grown under the Zn-rich condition, in which most doped Ag atoms are expected to occupy the O sites.[44,45] In this situation, n-type is formed, and electron concentration can be further increased for further reducing the resistivity of GaZnO NNs. The Hall measurement results, including electron concentration, mobility, and resistivity, of GaZnO thin films of ~300 nm in thickness grown with the substrate temperatures at 250, 350, and 450 °C on GaN templates are listed in Table 4. Here, one can see the large differences of electron concentration and resistivity between the GaZnO thin films grown at 350 and 450 °C. Although it is difficult to directly measure the electrical property of a GaZnO NN, its resistivity is expected to be about the same as or even better than that in a thin film since their Ga contents are about the same and an NN is doped with Ag. The large difference in field emission behavior between the NN samples grown at 350 and 450 °C is mainly caused by the difference of their electron concentrations. It is noted that, from the discussions above, one can conclude that the temperature

Table 4. Hall Measurement Results, Including Electron Concentration, Mobility, and Resistivity, of GaZnO Thin Films of ~300 nm in Thickness Grown with the Substrate Temperatures 250, 350, and 450 °C on GaN Templates

	GaZnO grown at 250 °C	GaZnO grown at 350 °C	GaZnO grown at 450 °C
electron conc (cm^{-3})	1.1 × 10^{21}	8.0 × 10^{20}	1.3 × 10^{20}
mobility [cm^2/(V s)]	29	31	14
resistivity (Ω cm)	1.8 × 10^{-4}	2.5 × 10^{-4}	3.0 × 10^{-3}

Table 3. Comparisons of Turn-On Electric Field, Threshold Electric Field, and Field Enhancement Factor between This Work under Two Growth Conditions and the Cited Accomplishments of Other Materials

	graphene[20]	CNT + Ag NP[13]	NdB_6[25]	ZnO[27]	this work (350 °C)	this work (450 °C)
turn-on electrical field, E_{on} (V/μm)	1.3	0.3	2.7	1.3	0.18	3.83
threshold electrical field, E_{th} (V/μm)	3.0	0.42	3.6	2.9	0.30	4.41
field enhancement factor, β	1.1 × 10^4	3.0 × 10^4	368	1.4 × 10^4	5.0 × 10^4	2072

DOI: 10.1021/acsami.5b02063
ACS Appl. Mater. Interfaces 2015, 7, 10525–10533

for melting a portion of a Ag NP with the size range shown in Figure 1a for VLS growth is between 250 and 350 °C. If the Ag NP size can be reduced, GaZnO NNs can be grown at a lower temperature. In this situation, as shown in Table 4, the electron concentration and hence the conductivity in the GaZnO NNs can be further enhanced. For field emission application, besides the high conductivity and high field enhancement factor of an NN, the NN geometry and density are also important factors. Such factors are controlled by the Ag NP distribution. A smaller Ag NP can be used for growing a narrower NN. A higher Ag NP density can result in a higher NN density for increasing emitted current.

6. CONCLUSIONS

In summary, we have demonstrated the MBE growth of GaZnO NNs based on the VLS growth mode using Ag NPs as the growth catalyst. It was shown that when the growth substrate temperature was high enough, a portion of a Ag NP could be melted for serving as the catalyst to precipitate GaZnO on the residual Ag NP and form a GaZnO NN. Record-low turn-on and threshold electric fields in the field emission test of the grown GaZnO NNs were observed. Also, a record-high field enhancement factor was calibrated. Such superior field emission performances were attributed to a few factors, including (1) the low work function and high conductivity of the grown GaZnO NNs due to highly degenerate Ga doping, (2) the sharp-pointed geometry of the vertically aligned GaZnO NNs, (3) the Ag doping in VLS precipitation of GaZnO for further reducing NN resistivity, and (4) the residual small Ag NP at the NN tip for making the tip even sharper and tip conductivity even higher. It should be emphasized that the Ag doping in GaZnO and the formation of a Ag NP at the NN tip were achieved naturally through the VLS growth of GaZnO NNs.

AUTHOR INFORMATION

Corresponding Author

*E-mail: ccycc@ntu.edu.tw.

Author Contributions

The paper was written through contributions of all authors. All authors have given approval to the final version of the paper.

Notes

The authors declare no competing financial interest.

ACKNOWLEDGMENTS

This research was supported by Ministry of Science and Technology, Taiwan, The Republic of China, under the grants of MOST 103-2120-M-002-002, NSC 102-2221-E-002-204-MY3, and MOST 103-2221-E-002-139, by the Excellent Research Projects of National Taiwan University (103R890951 and 103R890952), and by the US Air Force Scientific Research Office under the contract of AOARD-14-4105.

REFERENCES

(1) Nomura, K.; Ohta, H.; Takagi, A.; Kamiya, T.; Hirano, M.; Hosono, H. Room-temperature Fabrication of Transparent Flexible Thin-film Transistors Using Amorphous Oxide Semiconductors. *Nature* **2004**, *432*, 488−492.

(2) Liu, H.; Avrutin, V.; Izyumskaya, N.; Özgür, Ü.; Morkoç, H. Transparent Conducting Oxides for Electrode Applications in Light Emitting and Absorbing Devices. *Superlattices Microstruct.* **2010**, *48*, 458−484.

(3) Tadatsugu, M. Transparent Conducting Oxide Semiconductors for Transparent Electrodes. *Semicond. Sci. Technol.* **2005**, *20*, S35−S44.

(4) Exarhos, G. J.; Zhou, X.-D. Discovery-based Design of Transparent Conducting Oxide Films. *Thin Solid Films* **2007**, *515*, 7025−7052.

(5) Agura, H.; Suzuki, A.; Matsushita, T.; Aoki, T.; Okuda, M. Low Resistivity Transparent Conducting Al-doped ZnO Films Prepared by Pulsed Laser Deposition. *Thin Solid Films* **2003**, *445*, 263−267.

(6) Suzuki, A.; Matsushita, T.; Wada, N.; Sakamoto, Y.; Okuda, M. Transparent Conducting Al-Doped ZnO Thin Films Prepared by Pulsed Laser Deposition. *Jpn. J. Appl. Phys.* **1996**, *35*, L56−L59.

(7) Bhosle, V.; Tiwari, A.; Narayan, J. Electrical Properties of Transparent and Conducting Ga Doped ZnO. *J. Appl. Phys.* **2006**, *100*, 033713.

(8) Ken, N.; Kentaro, T.; Mitsuhiko, S.; Daisuke, N.; Norikazu, I.; Masayuki, S.; Hidemi, T.; Hitoshi, T.; Paul, F.; Koji, M.; Kakuya, I.; Akimasa, Y.; Shigeru, N. Improved External Efficiency InGaN-Based Light-Emitting Diodes with Transparent Conductive Ga-Doped ZnO as p-Electrodes. *Jpn. J. Appl. Phys.* **2004**, *43*, L180−L182.

(9) Zhao, J. L.; Sun, X. W.; Ryu, H.; Moon, Y. B. Thermally Stable Transparent Conducting and Highly Infrared Reflective Ga-doped ZnO Thin Films by Metal Organic Chemical Vapor Deposition. *Opt. Mater.* **2011**, *33*, 768−772.

(10) Shin, S. W.; Sim, K. U.; Moon, J.-H.; Kim, J. H. The Effect of Processing Parameters on The Properties of Ga-doped ZnO Thin Films by RF Magnetron Sputtering. *Curr. Appl. Phys.* **2010**, *10*, S274−S277.

(11) Fowler, R. H.; Nordheim, L. Electron Emission in Intense Electric Fields. *Proc. R. Soc. London, Ser. A* **1928**, *119*, 173−181.

(12) Xu, C. X.; Sun, X. W.; Chen, B. J. Field Emission From Gallium-doped Zinc Oxide Nanofiber Array. *Appl. Phys. Lett.* **2004**, *84*, 1540−1542.

(13) Ye, Y.; Guo, T. Effect of MWNT Electroless Ag Plating on Field Emission Properties of MWNT/Ag Nanocomposite Cathodes. *Appl. Surf. Sci.* **2013**, *264*, 593−597.

(14) Ye, C.; Bando, Y.; Fang, X.; Shen, G.; Golberg, D. Enhanced Field Emission Performance of ZnO Nanorods by Two Alternative Approaches. *J. Phys. Chem. C* **2007**, *111*, 12673−12676.

(15) Chang, L. W.; Yeh, J. W.; Cheng, C. L.; Shieu, F. S.; Shih, H. C. Field Emission and Optical Properties of Ga-doped ZnO Nanowires Synthesized via Thermal Evaporation. *Appl. Surf. Sci.* **2011**, *257*, 3145−3151.

(16) Zhu, W. *Vacuum Microelectronics*; John Wiley & Sons, Inc.: New York, 2001.

(17) Fan, S.; Chapline, M. G.; Franklin, N. R.; Tombler, T. W.; Cassell, A. M.; Dai, H. Self-Oriented Regular Arrays of Carbon Nanotubes and Their Field Emission Properties. *Science* **1999**, *283*, 512−514.

(18) Kan, M. C.; Huang, J. L.; Sung, J. C.; Chen, K. H.; Yau, B. S. Thermionic Emission of Amorphous Diamond and Field Emission of Carbon Nanotubes. *Carbon* **2003**, *41*, 2839−2845.

(19) Ahmed, S. F.; Das, S.; Mitra, M. K.; Chattopadhyay, K. K. Effect of Temperature on the Electron Field Emission from Aligned Carbon Nanofibers and Multiwalled Carbon Nanotubes. *Appl. Sur. Sci.* **2007**, *254*, 610−615.

(20) Jiang, L.; Yang, T.; Liu, F.; Dong, J.; Yao, Z.; Shen, C.; Deng, S.; Xu, N.; Liu, Y.; Gao, H. J. Controlled Synthesis of Large-Scale, Uniform, Vertically Standing Graphene for High-Performance Field Emitters. *Adv. Mater.* **2013**, *25*, 250−255.

(21) Li, J.; Chen, J.; Shen, B.; Yan, X.; Xue, Q. Temperature Dependence of the Field Emission from the Few-layer Graphene Film. *Appl. Phys. Lett.* **2011**, *99*, 163103.

(22) Koh, A. T. T.; Foong, Y. M.; Yusop, Z.; Tanemura, M.; Chua, D. H. C. Low Temperature Direct of Graphene onto Metal Nano-Spindt Tip with Applications in Electron Emission. *Adv. Mater. Interfaces* **2014**, *1*, 1300147.

(23) Zhang, H.; Tang, J.; Zhang, Q.; Zhao, G.; Yang, G.; Zhang, J.; Zhou, O.; Qin, L. C. Field Emission of Electrons from Single LaB_6 Nanowires. *Adv. Mater.* **2006**, *18*, 87−91.

DOI: 10.1021/acsami.5b02063
ACS Appl. Mater. Interfaces 2015, 7, 10525−10533

(24) Zhang, Q. Y.; Xu, J. Q.; Zhao, Y. M.; Ji, X. H.; Lau, S. P. Fabrication of Large-Scale Single-Crystalline PrB_6 Nanorods and Their Temperature-Dependent Electron Field Emission. *Adv. Funct. Mater.* **2009**, *19*, 742−747.
(25) Xu, J.; Hou, G.; Mori, T.; Li, H.; Wang, Y.; Chang, Y.; Luo, Y.; Yu, B.; Ma, Y.; Zhai, T. Excellent Field-Emission Performances of Neodymium Hexaboride (NdB_6) Nanoneedles with Ultra-Low Work Functions. *Adv. Funct. Mater.* **2013**, *23*, 5038−5048.
(26) Zhu, Y. W.; Zhang, H. Z.; Sun, X. C.; Feng, S. Q.; Xu, J.; Zhao, Q.; Xiang, B.; Wang, R. M.; Yu, D. P. Efficient Field Emission from ZnO Nanoneedle Arrays. *Appl. Phys. Lett.* **2003**, *83*, 144−146.
(27) Wang, W. Z.; Zeng, B. Q.; Yang, J.; Poudel, B.; Huang, J. Y.; Naughton, M. J.; Ren, Z. F. Aligned Ultralong ZnO Nanobelts and Their Enhanced Field Emission. *Adv. Mater.* **2006**, *18*, 3275−3278.
(28) Zhao, Q.; Xu, X. Y.; Song, X. F.; Zhang, X. Z.; Yu, D. P.; Li, C. P.; Guo, L. Enhanced Field Emission from ZnO Nanorods via Thermal Annealing in Oxygen. *Appl. Phys. Lett.* **2006**, *88*, 033102.
(29) Lee, C. J.; Lee, T. J.; Lyu, S. C.; Zhang, Y.; Ruh, H.; Lee, H. J. Field Emission from Well-aligned Zinc Oxide Nanowires Grown at Low Temperature. *Appl. Phys. Lett.* **2002**, *81*, 3648−3650.
(30) Xue, X. Y.; Li, L. M.; Yu, H. C.; Chen, Y. J.; Wang, Y. G.; Wang, T. H. Extremely Stable Field Emission from AlZnO Nanowire Arrays. *Appl. Phys. Lett.* **2006**, *89*, 043118.
(31) Ahmad, M.; Sun, H.; Zhu, J. Enhanced Photoluminescence and Field-Emission Behavior of Vertically Well Aligned Arrays of In-Doped ZnO Nanowires. *ACS Appl. Mater. Interfaces* **2011**, *3*, 1299−1305.
(32) Chu, F. H.; Huang, C. W.; Hsin, C. L.; Wang, C. W.; Yu, S. Y.; Yeh, P. H.; Wu, W. W. Well-aligned ZnO Nanowires with Excellent Field Emission and Photocatalytic Properties. *Nanoscale* **2012**, *4*, 1471−1475.
(33) Chiu, H. M.; Tsai, H. J.; Hsu, W. K.; Wu, J. M. Experimental and Computational Insights in the Growth of Gallium-doped Zinc Oxide Nanostructures with Superior Field Emission Properties. *CrystEngComm* **2013**, *15*, 5764−5775.
(34) Hsu, C. L.; Su, C. W.; Hsueh, T. J. Enhanced Field Emission of Al-doped ZnO Nanowires Grown on a Flexible Polyimide Substrate with UV Exposure. *RSC Adv.* **2014**, *4*, 2980−2983.
(35) Wagner, R. S.; Ellis, W. C. Vapor-liquid-solid Mechanism of Single Crystal Growth. *Appl. Phys. Lett.* **1964**, *4*, 89−90.
(36) Kuykendall, T.; Pauzauskie, P. J.; Zhang, Y.; Goldberger, J.; Sirbuly, D.; Denlinger, J.; Yang, P. Crystallographic Alignment of High-density Gallium Nitride Nanowire Arrays. *Nat. Mater.* **2004**, *3*, 524−528.
(37) Tang, T. Y.; Shiao, W. Y.; Lin, C. H.; Shen, K. C.; Huang, J. J.; Ting, S. Y.; Liu, T. C.; Yang, C. C.; Yao, C. L.; Yeh, J. H.; Hsu, T. C.; Chen, W. C.; Hsu, H. C.; Chen, L. C. Coalescence Overgrowth of GaN Nanocolumns on Sapphire with Patterned Metal Organic Vapor Phase Epitaxy. *J. Appl. Phys.* **2009**, *105*, 023501.
(38) Yamada, T.; Makino, H.; Yamamoto, N.; Yamamoto, T. Ingrain and Grain Boundary Scattering Effects on Electron Mobility of Transparent Conducting Polycrystalline Ga-doped ZnO Films. *J. Appl. Phys.* **2010**, *107*, 123534.
(39) Choi, K. H.; Jeon, S.; Kim, H. K. A Comparison of Ga:ZnO and Ga:ZnO/Ag/Ga:ZnO Source/Drain Electrodes for In-Ga-Zn-O Thin Film Transistors. *Mater. Res. Bull.* **2012**, *47*, 2915−2918.
(40) Song, J.; Kulinich, S. A.; Yan, J.; Li, Z.; He, J.; Kan, C.; Zeng, H. Epitaxial ZnO Nanowire-on-Nanoplate Structures as Efficient and Transferable Field Emitters. *Adv. Mater.* **2013**, *25*, 5750−5755.
(41) Zhai, T.; Li, L.; Ma, Y.; Liao, M.; Wang, X.; Fang, X.; Yao, J.; Bando, Y.; Golberg, D. One-dimensional Inorganic Nanostructures: Synthesis, Field-Emission and Photodetection. *Chem. Soc. Rev.* **2011**, *40*, 2986−3004.
(42) Deng, R.; Yao, B.; Li, Y. F.; Yang, T.; Li, B. H.; Zhang, Z. Z.; Shan, C. X.; Zhang, J. Y.; Shen, D. Z. Influence of Oxygen/Argon Ratio on Structural, Electrical and Optical Properties of Ag-doped ZnO Thin Films. *J. Cryst. Growth* **2010**, *312*, 1813−1816.
(43) Chiu, H. M.; Chang, Y. T.; Wu, W. W.; Wu, J. M. Synthesis and Characterization of One-Dimensional Ag-Doped ZnO/Ga-Doped ZnO Coaxial Nanostructure Diodes. *ACS Appl. Mater. Interfaces* **2014**, *6*, 5183−5191.
(44) Demchenko, D. O.; Earles, B.; Liu, H. Y.; Avrutin, V.; Izyumskaya, N.; Özgür, Ü.; Morkoç, H. Impurity Complexes and Conductivity of Ga-doped ZnO. *Phys. Rev. B* **2011**, *84*, 075201.
(45) Li, Y.; Zhao, X.; Fan, W. Structural, Electronic, and Optical Properties of Ag-Doped ZnO Nanowires: First Principles Study. *J. Phys. Chem. C* **2011**, *115*, 3552−3557.

DOI: 10.1021/acsami.5b02063
ACS Appl. Mater. Interfaces 2015, 7, 10525−10533